The proton donor for O—O bond scission by cytochrome *c* oxidase

Elena A. Gorbikova, Ilya Belevich, Mårten Wikström, and Michael I. Verkhovsky*

Helsinki Bioenergetics Group, Institute of Biotechnology, University of Helsinki, P.O. Box 65 Viikinkaari 1, FI-00014, Helsinki, Finland

Edited by Harry B. Gray, California Institute of Technology, Pasadena, CA, and approved June 16, 2008 (received for review March 12, 2008)

Cytochrome *c* oxidase is the main catalyst of oxygen consumption in mitochondria and many aerobic bacteria. The key step in oxygen reduction is scission of the O—O bond and formation of an intermediate P_R of the binuclear active site composed of heme a_3 and Cu_B. The donor of the proton required for this reaction has been suggested to be a unique tyrosine residue (Tyr-280) covalently cross-linked to one of the histidine ligands of Cu_B. To test this idea we used the Glu-278–Gln mutant enzyme from *Paracoccus denitrificans*, in which the reaction with oxygen stops at the P_R intermediate. Three different time-resolved techniques were used. Optical spectroscopy showed fast (≈60 μs) appearance of the P_R species along with full oxidation of heme *a*, and FTIR spectroscopy revealed a band at 1,308 cm^{-1}, which is characteristic for the deprotonated form of the cross-linked Tyr-280. The development of electric potential during formation of the P_R species suggests transfer of a proton over a distance of ≈4 Å perpendicular to the membrane plane, which is close to the distance between the oxygen atom of the hydroxyl group of Tyr-280 and the bound oxygen. These results strongly support the hypothesis that the cross-linked tyrosine is the proton donor for O—O bond cleavage by cytochrome *c* oxidase and strengthens the view that this tyrosine also provides the fourth electron in O_2 reduction in conditions where heme *a* is oxidized.

His/Tyr dimer | cytochrome aa_3 | cell respiration | proton transfer | FTIR spectroscopy

The electrons required for oxygen reduction by cytochrome *c* oxidase (C*c*O) take a specific route from the water-soluble electron donor, cytochrome *c*, via Cu_A and heme *a* to the binuclear heme a_3/Cu_B center where O_2 is bound. The energy released during the overall reaction is used for proton translocation across the mitochondrial or bacterial membrane (1). The catalytic cycle of C*c*O starts with binding of dioxygen to heme a_3 [formation of a ferrous O_2 adduct, compound **A** (2)]. This step is followed by scission of the O—O bond, which requires delivery of four electrons and a proton to dioxygen and leaves the binuclear site in the highly oxidized **P** state (3-5). Three of the four required electrons are donated by heme a_3 (two electrons) and Cu_B (one electron). The source of the fourth electron depends on the initial reduction level of the enzyme. When catalysis starts from the fully reduced enzyme, the fourth electron is provided by heme *a* and the so-called $\mathbf{P_R}$ state is formed at the binuclear site (6-9). When the reaction with oxygen starts from the mixed-valence (two-electron reduced) enzyme where both heme *a* and Cu_A are oxidized, a **P** state is also formed (called $\mathbf{P_M}$), and the fourth required electron is in this case thought to be donated by a nearby amino acid residue. The optical spectrum of $\mathbf{P_M}$ is indistinguishable from $\mathbf{P_R}$ (9), which indicates that the binuclear heme a_3 /Cu_B site has a similar structure in these intermediates. Scission of the O—O bond also requires delivery of a proton; in both the "fully reduced" and "mixed-valence" cases this proton is taken from a nearby residue, because there is no proton uptake from the medium (10), and only a small electrometric signal is observed arising from internal proton transfer (ref. 11 and see below).

The oxygen atom of the hydroxyl group of Tyr-280 (*Paracoccus denitrificans* numbering) is located at a distance of ≈5.7 Å from Cu_B (12, 13), which makes it a reasonable candidate as the local proton donor (Fig. 1). The conserved Tyr-280 has attracted special attention because of its posttranslational modification that results in a covalent cross-link to one of the histidine ligands of Cu_B (14-16), namely His-276. This cross-link connects the C6 atom of the tyrosine and the ε-nitrogen of the histidine. As shown for a model compound of the His/Tyr dimer, the cross-link lowers the pK_a of the tyrosine from ≈10 to ≈8.5 (17-19), thus facilitating donation of a proton. The cross-linked tyrosine has also been proposed to be the donor of the fourth electron in the oxygen reaction of the mixed-valence enzyme (3, 20), thus forming a neutral radical. Infrared properties of the cross-linked His/Tyr model compound in protonated, deprotonated, and neutral radical forms were defined earlier (19, 21). Moreover, several infrared absorption bands of the cross-linked Tyr-280 were identified in difference spectra of C*c*O from *P. denitrificans* by applying specific isotopic labeling (22).

To test the proposed role of the cross-linked Tyr-280 as the donor of the proton for O—O bond cleavage, we applied a combination of time-resolved visible spectroscopy, Fourier transform infrared (FTIR) spectroscopy, and electrometry. The reaction of oxygen with the fully reduced Glu-278–Gln variant of C*c*O was studied, in which the key residue of the proton translocation process is mutated so that the reactions beyond the $\mathbf{P_R}$ intermediate become extremely slow.

Results

Formation of the P_R Intermediate in the Glu-278–Gln Mutant Enzyme. Time-resolved optical spectroscopy was applied to monitor the reaction of the fully reduced CO-inhibited (**FRCO**) Glu-278–Gln mutant enzyme with oxygen. From this approach the complete surface (absorption, wavelength, time) was obtained in the 380- to 820-nm wavelength range. Kinetic traces of the reaction at selected wavelengths are shown in Fig. 2*A*. An immediate absorbance jump, best seen at 445 nm, corresponds to photodissociation of CO and occurs within 1 μs. CO dissociation is followed by phases caused by the reaction with oxygen. A global fit of the data to a two-step sequential model revealed a phase with τ (time constant = $1/k$, where k is the rate constant) ≈8.5 μs, characterized by peaks at 416 and 595 nm and troughs at 446, 570, and 618 nm (Fig. 2*B*, black, τ_1). This phase can be assigned to the **R** (fully reduced) → **A** transition, i.e., to formation of the primary oxygen adduct (23, 24). Compound **A** is unstable, and in the Glu-278–Gln variant it relaxes with τ_2 ≈53 μs to a species with peaks at 413 and 620 nm and troughs at 444 and 599 nm (Fig. 2*B*, gray). Based on these optical features (9), we can assign the 53-μs phase to the $\mathbf{A} \rightarrow \mathbf{P_R}$ transition. No Cu_A oxidation was detected on the time scale of $\mathbf{P_R}$ formation (Fig. 2*A*, trace at 820 nm) (see also ref. 25), whereas heme *a* becomes fully oxidized.

Relaxation of the P_R intermediate in the Glu-278–Gln Mutant Enzyme. In the Glu-278–Gln variant the oxygen reaction is strongly inhibited after formation of the $\mathbf{P_R}$ intermediate (25, 26), which allows a study

Author contributions: E.A.G. and M.I.V. designed research; E.A.G. and I.B. performed research; E.A.G., I.B., M.W., and M.I.V. analyzed data; and E.A.G., I.B., M.W., and M.I.V. wrote the paper.

The authors declare no conflict of interest.

This article is a PNAS Direct Submission.

*To whom correspondence should be addressed. E-mail: michael.verkhovsky@helsinki.fi.

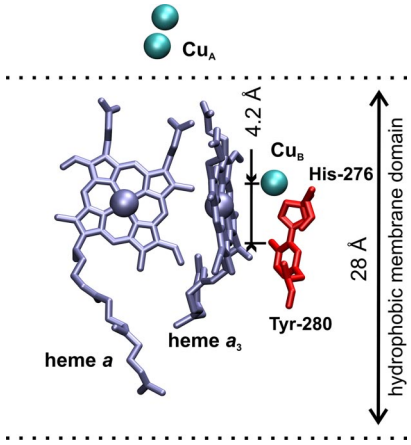

Fig. 1. Location of redox centers of C*c*O: heme *a* and heme a_3 (silver), Cu_B and Cu_A (cyan spheres), and the His-276/Tyr-280 dimer (red) within the hydrophobic part of the membrane. The membrane dielectric thickness (≈28 Å) and the distance between the oxygen atoms of the hydroxyl groups of Tyr-280 and Cu_B projected on the membrane normal (≈4.2 Å) are marked. The figure was prepared from the bovine structure 2DYR (13) by using VMD software (47).

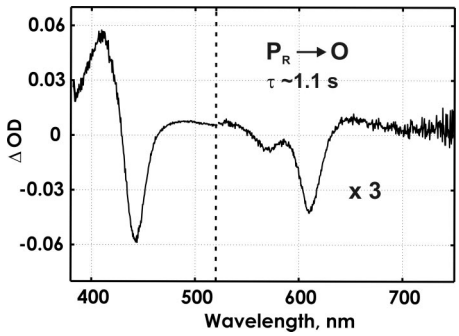

Fig. 3. The spectrum of the kinetic component (the $P_R \rightarrow O$ transition) of the oxygen reaction in the ATR sample of the Glu-278–Gln mutant enzyme obtained in the reflectance mode on a millisecond time scale. Conditions were: K-phosphate buffer, 200 mM (pH 6); hexaammineruthenium, 10–20 μM; glucose, 100 mM; catalase, 260 mg/ml; glucose oxidase, 670 mg/ml; K-ascorbate, 3.3 mM; CO, 100%. The reaction was started by a laser flash ≈350 ms after the beginning of the injection of 100 μl of oxygen-saturated buffer.

of the early reaction by FTIR spectroscopy in the attenuated total reflectance (ATR) mode on enzyme film immobilized on the ATR prism (see *Materials and Methods*) (27). The reaction can be followed simultaneously by FTIR and visible spectroscopy with our current flow-flash setup. Even though the time resolution of the visible spectrophotometer used here (1 ms between the spectra) and the FTIR spectrometer in rapid-scan mode (≈46 ms) is not high enough to resolve the fast steps of the reaction, the slow steps after $\mathbf{P_R}$ formation can be probed in the mutant enzyme. The time-resolved kinetics in the visible range, after an immediate jump within 1 ms, shows a single phase with $\tau \approx 1.1$ s (Fig. 3), which corresponds to disappearance of the $\mathbf{P_R}$ intermediate (troughs at 439, 608, and 568 nm) and simultaneous appearance of the **O** (fully oxidized) state (peaks at 409 and 660 nm) (28,29) without detectable formation of the ferryl intermediate (**F**). The spectrum of the $\mathbf{P_R} \rightarrow \mathbf{O}$ transition shows no heme *a* oxidation, which agrees with full oxidation already during formation of $\mathbf{P_R}$ (see above).

Infrared Properties of the P_R Intermediate. The Glu-278–Gln variant serves as a good tool to monitor the infrared properties of the $\mathbf{P_R}$ intermediate because the oxygen reaction is virtually stopped after formation of this state. The active site of the mutant enzyme, immobilized on the ATR prism, was not disturbed, as confirmed by an unchanged rate of CO recombination ($\tau \approx 18$ ms, as measured by visible spectroscopy) compared with the WT enzyme in solution (30). A total of 118 time-resolved FTIR surfaces of the reaction with oxygen were then collected and averaged. The resulting surface showed two reaction-related features. An immediate absorbance jump may be assigned to the unresolved processes that occur faster than the resolution of our measurements (46 ms) and include CO photodissociation together with formation of the **A** and $\mathbf{P_R}$ intermediates. The FTIR spectrum of this step, i.e., the **FRCO** $\rightarrow \mathbf{P_R}$ transition, is shown in Fig. 4. The subsequent infrared absorbance changes have a time constant of ≈1 s and correspond to the optically detected $\mathbf{P_R} \rightarrow \mathbf{O}$ transition. The sum of the spectra of the unresolved jump and the 1-s kinetic phase gives a spectrum (data not shown) very similar to the spectrum of the **FRCO** $\rightarrow$ **O** transition (27), which confirms the optical data, and shows that the $\mathbf{P_R}$ intermediate indeed relaxes to the **O** state.

The FTIR spectrum of the **FRCO** $\rightarrow \mathbf{P_R}$ transition shows the appearance of a band at 1,308 cm^{-1} (Fig. 4) with a half-width of ≈20 cm^{-1} that correlates with oxidation of Cu_B (31). It should be noted that the spectrum of photolysis gives itself no contribution at the position ≈1,308 cm^{-1} (ref. 32 and unpublished data). A similar band was also found in the spectrum of a deprotonated cross-linked His/Tyr model compound, showing prominent peaks centered at ≈1,508, 1,480, and 1,305 cm^{-1} that disappear both in the protonated and neutral radical forms (19, 21). Also, Iwaki *et al.* (22) found three bands in the **O** state relative to $\mathbf{P_M}$ of C*c*O from *P. denitrificans* (at 1,506, 1,311, and 1,094 cm^{-1}), which are sensitive to isotope labeling of both tyrosine and histidine and assigned to the cross-

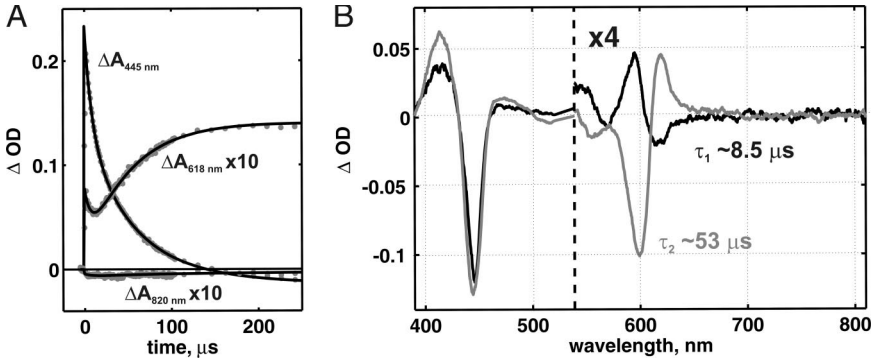

Fig. 2. The oxygen reaction of the Glu-278–Gln mutant enzyme followed by time-resolved visible spectroscopy. (*A*) Kinetics of optical changes at 445, 618, and 820 nm. (*B*) The difference spectra of the 8.5-μs kinetic phase ($R \rightarrow A$) in black and the 53-μs phase ($A \rightarrow P_R$) in gray. Conditions after mixing were: C*c*O, 1.75 μM; Mops, 17 mM (pH 7); TMPD (*N*,*N*,*N*′,*N*′-tetramethyl-1,4-phenylenediamine), 0.8 μM; K-ascorbate, 0.8 μM; oxygen, 1.1 mM. The reaction was started by a laser flash 5 ms after mixing the enzyme solution with oxygen-saturated buffer in the ratio 1:5.

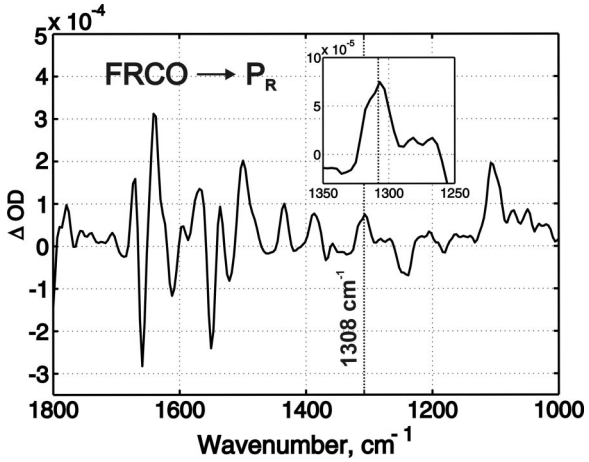

Fig. 4. The kinetic FTIR spectrum of the FRCO → P_R transition measured with the Glu-278–Gln mutant enzyme. Conditions were the same as in Fig. 3 except that the reaction was started by a laser flash 3 s from the beginning of injection of 100 μl of oxygen-saturated buffer. (*Inset*) An enlarged view of the region around the band at 1,308 cm^{-1}. The concentration of active enzyme was ≈0.3 mM.

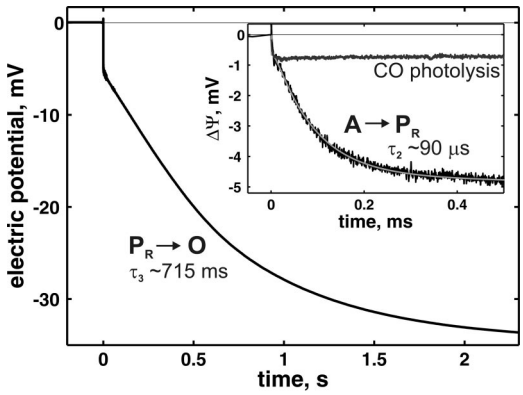

Fig. 5. Membrane potential generation ($\Delta\Psi$) during the oxygen reaction of the Glu-278–Gln variant as detected by time-resolved electrometry. The experimental data shows the mean of three experiments (black) and are plotted together with the theoretical fit (gray). Conditions were: Mops-KOH, 100 mM (pH 7); hexaammineruthenium, 100 nM; glucose, 50 mM; catalase, 0.3 mg/ml; glucose oxidase, 3 mg/ml; CO, 100%. The reaction was started by a laser flash 1.4 s after the beginning of the injection of 100 μl of oxygen-saturated buffer. (*Inset*) The same trace together with the potential generation upon CO photodissociation without oxygen addition on a shorter time scale. The experimental traces were scaled by the amplitude of CO photodissociation phase to match the WT enzyme.

linked His/Tyr dimer, being most likely in the deprotonated form. The trough at 1,311 cm^{-1} in ref. 22 showed the same half-width as the peak at 1,308 cm^{-1} in Fig. 4. From this comparison we conclude that the peak at 1,308 cm^{-1} very likely belongs to Tyr-280 that becomes deprotonated on formation of the $\mathbf{P_R}$ state. The same band with full amplitude normalized to the amplitude of CO photolysis was also detected in the spectra of the **FRCO** → **F** and **FRCO** → **O** transitions in alkaline conditions (27), suggesting full deprotonation of the tyrosine in the **F** and **O** states (*cf.* ref. 21 and see below). The other two bands assigned to the deprotonated His/Tyr dimer (at 1,506 and 1,094 cm^{-1}) are not discerned in our spectra, presumably because of strong overlapping bands in these spectral regions.

Charge Transfer Across the Membrane Dielectric During Formation of the P_R Intermediate. An independent test of proton donation for O—O bond cleavage can be done by following the oxygen reaction by time-resolved electrometry in vesicles with reconstituted enzyme. The electrometric technique is a sensitive probe for the determination of the distance of electrical charge movement in the direction perpendicular to the membrane plane (33). The proton delivered for O—O bond cleavage should create a potential proportional to the distance between the binuclear center and the proton donor. The oxygen reaction of the Glu-278–Gln variant showed an electrometric response with small amplitude (Fig. 5) compared with the WT enzyme in identical conditions. However, the mutant enzyme forms a smaller amount of CO adduct before the reaction, which should be taken into account. Photolysis of **FRCO** results in very fast ($\tau \approx 1$ μs) generation of electric potential negative inside (Fig. 5 *Inset*, CO photodissociation trace) caused by coupled movement of dipoles or possible charge redistribution upon relaxation of the binuclear center. The amplitude of this potential generation is proportional to the amount of photolyzed sample and can thus be used to normalize the amplitude in the reaction of the reduced enzyme with oxygen for different samples. The reconstitution procedure used in this work results in a mean potential generation of 0.81 ± 0.08 mV (n = 17) caused by CO photodissociation in the WT C*c*O, which corresponds to 109 ± 5.3 mV generated during the oxygen reaction for the same samples. For the Glu-278–Gln mutant enzyme the amplitude caused by CO photodissociation was only 0.4 ± 0.1 mV at the same enzyme concentration. Fig. 5 shows the mean of three experiments where potential generation was measured during the oxygen reaction of the Glu-278–Gln mutant enzyme, scaled by the CO photodissociation phase to match the response in WT enzyme.

The electrometric response may be fitted in the same way as the visible optical data (Fig. 5), by two fast and one slow reaction step: the first step is a nonelectrogenic transition (τ_1 ≈8.3 μs) that corresponds to formation of compound **A**, and the second is an electrogenic phase that develops with τ_2 ≈90 μs with an amplitude of 3.9 ± 2.1 mV (Fig. 5 *Inset*, τ_2). We assign this latter step to the **A** → $\mathbf{P_R}$ transition, because a similar rate constant was detected by visible spectroscopy (see above). A third slow phase has a time constant of ≈715 ms and an amplitude of ≈30 mV (Fig. 5, τ_3) and correlates with the $\mathbf{P_R}$ → **O** reaction detected by visible spectroscopy (see above).

The development of electric potential during $\mathbf{P_R}$ formation in the Glu-278–Gln mutant can be caused by either electron or proton transfer that takes place perpendicular to the membrane plane. From the optical measurements we found that formation of $\mathbf{P_R}$ is coupled to electron transfer from heme *a* and Cu_B to dioxygen, but without any electron transfer from Cu_A (see above). Because the electron transfer between the hemes and Cu_B is electrometrically silent because of the location of these centers at the same depth in the membrane (12), we can assign the fast phase solely to proton transfer. However, there is no proton uptake from the external medium during $\mathbf{P_R}$ formation (34, 35). Formation of the $\mathbf{P_R}$ intermediate in the WT enzyme was proposed to be coupled to loading of a proton pump site by internal proton transfer from Glu-278 (36). However, in the Glu-278–Gln variant this group is mutated to glutamine and thus cannot donate the proton. Hence, the electrometrically detected charge transfer during **A** → $\mathbf{P_R}$ can here be solely attributed to an internal proton transfer in the direction toward the P-side of the membrane that is involved in cleavage of the O—O bond. If Tyr-280 is the proton donor for this reaction, then the amplitude of the electrometric response should correspond to the distance between Tyr-280 and dioxygen at the binuclear center, as projected on the membrane normal.

For the current typical reconstitution procedure (37), the full electrometric response of the oxygen reaction for WT C*c*O is 109 mV (see above). Considering that ≈3.7 charges are transferred across the membrane dielectric during this reaction (38), transfer of a single charge will yield an amplitude of 109/3.7, i.e., 29.5 mV. The

thickness of the hydrophobic barrier of the membrane is ≈28 Å (39) (Fig. 1); thus, the ≈3.9-mV mean response observed on $\mathbf{P_R}$ formation in the Glu-278–Gln variant corresponds to a distance of (3.9/29.5) × 28 = 3.7 ± 1.99 Å perpendicular to the membrane plane. The corresponding distance between the oxygen of Tyr-280 and the molecule of dioxygen at the binuclear center is ≈4.2 Å (Fig. 1). Considering the uncertainties in this calculation, the observed electrometric response is consistent with the notion of proton transfer from the hydroxyl of Tyr-280 to the oxygenous ligand of Cu_B during O—O bond scission.

Discussion

A key reaction in catalysis by C*c*O is the four-electron reduction of bound O_2 with rupture of the O—O bond, which requires transfer of four electrons and one proton. As discussed above, the proton donor must be located inside the enzyme, probably in close proximity of the binuclear center to provide the proton on the time scale of $\mathbf{P_R}$ formation. Both crystal structures (14, 40) and protein chemical analysis (14-16) have shown that Tyr-280 is cross-linked to a histidine ligand of Cu_B. This unique posttranslational modification and the location of Tyr-280 in the vicinity of the binuclear center suggested that this residue is the donor of the proton, and previous studies (3, 20, 22) support the proposal that Tyr-280 may also donate an electron on O—O bond cleavage in the mixed-valence enzyme. Nevertheless, the evidence of participation of the tyrosine in the oxygen reduction chemistry of C*c*O has remained inconclusive, and a direct assessment of the protonation state of Tyr-280 during this reaction is warranted. In this work we therefore characterized the formation of the $\mathbf{P_R}$ intermediate by time-resolved visible and FTIR spectroscopy, and electrometry. We chose a mutant in which the conserved Glu-278 was replaced by a nonprotonatable residue, because in this variant only the primary chemistry of O—O bond scission can happen, thereby isolating this event from other reactions.

The infrared spectrum of $\mathbf{P_R}$ formation shows a band at 1,308 cm^{-1}, which we assign to the cross-linked Tyr-280 based on infrared data on C*c*O after specific labeling of histidine and tyrosine (22) and particularly to its anionic form based on the spectra of the His/Tyr model compound (19, 21). The 1,308-cm^{-1} band is slightly shifted from the trough found in the $\mathbf{P_M}$-minus-**O** spectrum in the latter work [≈1,311 cm^{-1} (22)]. However, the **R**-minus-**O** spectrum reported in the same paper (22), where the reference state is comparable to our conditions, shows a trough at 1,308 cm^{-1} that shifts upon isotopic labeling of tyrosine. It should be noted that the CO stretching vibrations of a free tyrosine never exceeds a wavenumber of 1,280 cm^{-1} (41). The published $\mathbf{P_M}$-minus-**O** spectrum shows the isotope-sensitive 1,311-cm^{-1} band as a trough (22), indicating that it is a feature of the **O** state that is lacking or less prominent in $\mathbf{P_M}$. In contrast, generation of the $\mathbf{P_R}$ state from the reduced enzyme showed formation of the 1,308-cm^{-1} band (Fig. 4). From our previous work on the Asp-124–Asn variant it may be seen that this band remains fully developed in the **F** state, as well as in **O** under alkaline conditions (figure 4 in ref. 27). Hence, while this band is lacking from the $\mathbf{P_M}$ state (22), it is developed in the $\mathbf{P_R}$ species and stays with full amplitude in **F** and in state **O** under alkaline conditions. We therefore conclude that Tyr-280 is most likely in the neutral radical state in $\mathbf{P_M}$, as proposed previously, but that it is in the anionic state in $\mathbf{P_R}$. Our results therefore strongly support the idea that Tyr-280 is the proton donor in O—O bond scission, which also agrees with the notion that this residue provides both an electron and a proton when the mixed-valence enzyme reacts with O_2. If so, and in contrast to the fully reduced enzyme, this reaction should not generate electrical potential because the electron and the proton are transferred over the same distance in the same direction. Formation of the $\mathbf{P_M}$ state has indeed been found to be electroneutral (11), whereas electric potential development during formation of the $\mathbf{P_R}$ state is electrogenic with an amplitude that is consistent with our proposal. Recently, Lepp *et al.* (42) showed that mutations in the K-pathway of proton transfer slowed down formation of the $\mathbf{P_R}$ state. Although our electrometric data cannot exclude some additional charge reorganization in the K-pathway, it would have to be very small to be consistent with our observations. On the other hand, because Tyr-280 is located at the end of the K-pathway it seems quite possible that the effects reported in ref. 42 are caused by a rise in the pK_a of Tyr-280 by the used mutations, making it a poorer proton donor.

Materials and Methods

Enzyme Preparation. Site-directed mutagenesis, bacterial growth conditions, and purification of the Glu-278–Gln mutant of cytochrome aa_3 from *P. denitrificans* were as described (43).

Reaction of the Enzyme with Oxygen Followed by Visible Spectroscopy. The **FRCO** form of soluble C*c*O was mixed with oxygen-saturated buffer, after which CO was photodissociated by a laser flash to initiate the oxygen reaction. The fast phases of the reaction were measured by a CCD-based instrument (44) with a time resolution of 1 μs per spectrum. The oxygen reaction on a time scale from milliseconds to seconds was measured with the enzyme immobilized on the surface of the ATR prism (called the ATR sample), first described in (45). In this case, oxygen-saturated buffer was injected into the ATR sample, after which CO was photodissociated by a laser flash. The reaction was followed by using an HR2000+ spectrophotometer (27) with a time resolution of 1 ms per spectrum in the reflectance mode.

Reaction of the Enzyme with Oxygen Followed by FTIR Spectroscopy. The procedure of preparing the ATR sample and formation of the **FRCO** enzyme was essentially as described (27). CO recombination after photolysis was followed by visible spectroscopy to check the integrity of the binuclear center. CO photodissociation from heme a_3 after oxygen addition was followed by using the rapid-scan mode of the FTIR spectrometer IFS 66/s to estimate the concentration of active enzyme from the drop of amplitude of the band at 1,965 cm^{-1} (heme a_3 C ≡ O vibration). This test was followed by measuring the oxygen reaction. Oxygen-saturated buffer was injected to the ATR sample, followed by CO dissociation by the laser flash. Time-resolved FTIR measurements of the reaction were performed as described (27) in the rapid-scan mode with ≈46-ms time resolution in the range of 1,800 to 1,000 cm^{-1}, limited by a cut-off filter.

Reaction of the Enzyme with Oxygen Followed by Electrometry. Charge transfer across the membrane was monitored by an electrometric technique (33) as adapted for time-resolved experiments with C*c*O (11, 46). The Glu-278–Gln mutant enzyme was reconstituted into liposomes as described (37), and the oxygen reaction was initiated by a laser flash immediately after addition of oxygen. The electrometric response was measured with nanosecond time resolution.

The kinetic experiments on the ATR sample were done at ice-cooled conditions to decrease the reaction rates and increase the O_2 concentration up to ≈2.4 mM; otherwise the temperature was 21°C and the O_2 concentration was ≈1 mM.

Data Analysis. All data treatment and presentation was done with Matlab software.

ACKNOWLEDGMENTS. We thank Camilla Ribacka and Anne Puustinen for the production of the Glu-278–Gln mutant of C*c*O from *P. denitrificans*. This work was supported by Biocentrum Helsinki, the Sigrid Jusélius Foundation, and the Academy of Finland. E.A.G. was supported by the National Graduate School in Informational and Structural Biology.

1. Wikström MK (1977) Proton pump coupled to cytochrome *c* oxidase in mitochondria. *Nature* 266:271–273.
2. Babcock GT, Wikström M (1992) Oxygen activation and the conservation of energy in cell respiration. *Nature* 356:301–309.
3. Proshlyakov DA, Pressler MA, Babcock GT (1998) Dioxygen activation and bond cleavage by mixed-valence cytochrome *c* oxidase. *Proc Natl Acad Sci USA* 95:8020–8025.
4. Fabian M, Wong WW, Gennis RB, Palmer G (1999) Mass spectrometric determination of dioxygen bond splitting in the "peroxy" intermediate of cytochrome *c* oxidase. *Proc Natl Acad Sci USA* 96:13114–13117.

5. Proshlyakov DA, *et al.* (1994) Selective resonance Raman observation of the ''607 nm'' form generated in the reaction of oxidized cytochrome *c* oxidase with hydrogen peroxide. *J Biol Chem* 269:29385–29388.
6. Hill BC (1994) Modeling the sequence of electron transfer reactions in the single turnover of reduced, mammalian cytochrome *c* oxidase with oxygen. *J Biol Chem* 269:2419–2425.
7. Han SH, Ching YC, Rousseau DL (1990) Cytochrome *c* oxidase: Decay of the primary oxygen intermediate involves direct electron transfer from cytochrome *a*. *Proc Natl Acad Sci USA* 87:8408–8412.
8. Verkhovsky MI, Morgan JE, Wikström M (1994) Oxygen binding and activation: Early steps in the reaction of oxygen with cytochrome *c* oxidase. *Biochemistry* 33:3079–3086.
9. Morgan JE, Verkhovsky MI, Palmer G, Wikström M (2001) Role of the P-R intermediate in the reaction of cytochrome *c* oxidase with O-2. *Biochemistry* 40:6882–6892.
10. Oliveberg M, Hallen S, Nilsson T (1991) Uptake and release of protons during the reaction between cytochrome *c* oxidase and molecular oxygen: A flow-flash investigation. *Biochemistry* 30:436–440.
11. Jasaitis A, Verkhovsky MI, Morgan JE, Verkhovskaya ML, Wikström M (1999) Assignment and charge translocation stoichiometries of the major electrogenic phases in the reaction of cytochrome *c* oxidase with dioxygen. *Biochemistry* 38:2697–2706.
12. Iwata S, Ostermeier C, Ludwig B, Michel H (1995) Structure at 2.8-Å resolution of cytochrome *c* oxidase from *Paracoccus denitrificans*. *Nature* 376:660–669.
13. Muramoto K, *et al.* (2007) A histidine residue acting as a controlling site for dioxygen reduction and proton pumping by cytochrome *c* oxidase. *Proc Natl Acad Sci USA* 104:7881–7886.
14. Ostermeier C, Harrenga A, Ermler U, Michel H (1997) Structure at 2.7-Å resolution of the *Paracoccus denitrificans* two-subunit cytochrome *c* oxidase complexed with an antibody FV fragment. *Proc Natl Acad Sci USA* 94:10547–10553.
15. Yoshikawa S, Shinzawa-Itoh K, Tsukihara T (1998) Crystal structure of bovine heart cytochrome *c* oxidase at 2.8-Å resolution. *J Bionenerg Biomembr* 30:7–14.
16. Buse G, Soulimane T, Dewor M, Meyer HE, Bluggel M (1999) Evidence for a copper-coordinated histidine-tyrosine cross-link in the active site of cytochrome oxidase. *Protein Sci* 8:985–990.
17. McCauley KM, Vrtis JM, Dupont J, van der Donk WA (2000) Insights into the functional role of the tyrosine-histidine linkage in cytochrome *c* oxidase. *J Am Chem Soc* 122:2403–2404.
18. Aki M, *et al.* (2002) UV resonance Raman characterization of model compounds of Tyr(244) of bovine cytochrome *c* oxidase in its neutral, deprotonated anionic, and deprotonated neutral radical forms: Effects of covalent binding between tyrosine and histidine. *J Phys Chem A* 106:3436–3444.
19. Cappuccio JA, *et al.* (2002) Modeling the active site of cytochrorne oxidase: Synthesis and characterization of a cross-linked histidine-phenol. *J Am Chem Soc* 124:1750–1760.
20. Proshlyakov DA, *et al.* (2000) Oxygen activation and reduction in respiration: Involvement of redox-active tyrosine 244. *Science* 290:1588–1591.
21. Hellwig P, *et al.* (2002) Vibrational modes of tyrosines in cytochrome *c* oxidase from *Paracoccus denitrificans*: FTIR and electrochemical studies on Tyr-D-4-labeled and on Tyr-280–His and Tyr-35–Phe mutant enzymes. *Biochemistry* 41:9116–9125.
22. Iwaki M, Puustinen A, Wikström M, Rich PR (2006) Structural and chemical changes of the P-M intermediate of *Paracoccus denitrificans* cytochrome *c* oxidase revealed by IR spectroscopy with labeled tyrosines and histidine. *Biochemistry* 45:10873–10885.
23. Hill BC, Greenwood C (1984) The reaction of fully reduced cytochrome *c* oxidase with oxygen studied by flow-flash spectrophotometry at room temperature. Evidence for new pathways of electron transfer. *Biochem J* 218:913–921.
24. Verkhovsky MI, Morgan JE, Puustinen A, Wikström M (1996) The ''ferrous-oxy'' intermediate in the reaction of dioxygen with fully reduced cytochromes aa(3) and bo(3). *Biochemistry* 35:16241–16246.
25. Ädelroth P, Ek MS, Mitchell DM, Gennis RB, Brzezinski P (1997) Glutamate 286 in cytochrome aa(3) from *Rhodobacter sphaeroides* is involved in proton uptake during the reaction of the fully reduced enzyme with dioxygen. *Biochemistry* 36:13824–13829.
26. Verkhovskaya ML, *et al.* (1997) Glutamic acid 286 in subunit I of cytochrome bo(3) is involved in proton translocation. *Proc Natl Acad Sci USA* 94:10128–10131.
27. Gorbikova EA, Belevich NP, Wikström M, Verkhovsky MI (2007) Time-resolved ATR-FTIR spectroscopy of the oxygen reaction in the D124N mutant of cytochrome *c* oxidase from *Paracoccus denitrificans*. *Biochemistry* 46:13141–13148.
28. Siletsky S, Kaulen AD, Konstantinov AA (1999) Resolution of electrogenic steps coupled to conversion of cytochrome *c* oxidase from the peroxy to the ferryl-oxo state. *Biochemistry* 38:4853–4861.
29. Ribacka C, *et al.* (2005) An elementary reaction step of the proton pump is revealed by mutation of tryptophan-164 to phenylalanine in cytochrome *c* oxidase from *Paracoccus denitrificans*. *Biochemistry* 44:16502–16512.
30. Belevich I, Tuukkanen A, Wikström M, Verkhovsky MI (2006) Proton-coupled electron equilibrium in soluble and membrane-bound cytochrome *c* oxidase from *Paracoccus denitrificans*. *Biochemistry* 45:4000–4006.
31. Gorbikova EA, Vuorilehto K, Wikström M, Verkhovsky MI (2006) Redox titration of all electron carriers of cytochrome *c* oxidase by Fourier transform infrared spectroscopy. *Biochemistry* 45:5641–5649.
32. Rost B, *et al.* (1999) Time-resolved FT-IR studies on the CO adduct of *Paracoccus denitrificans* cytochrome *c* oxidase: Comparison of the fully reduced and the mixed valence form. *Biochemistry* 38:7565–7571.
33. Drachev LA, *et al.* (1974) Direct measurement of electric current generation by cytochrome oxidase, H+-ATPase and bacteriorhodopsin. *Nature* 249:321–324.
34. Hallen S, Nilsson T (1992) Proton transfer during the reaction between fully reduced cytochrome *c* oxidase and dioxygen: pH and deuterium isotope effects. *Biochemistry* 31:11853–11859.
35. Ädelroth P, Ek M, Brzezinski P (1998) Factors determining electron-transfer rates in cytochrome *c* oxidase: Investigation of the oxygen reaction in the *R. sphaeroides* enzyme. *Biochim Biophys Acta* 1367:107–117.
36. Belevich I, Verkhovsky MI, Wikström M (2006) Proton-coupled electron transfer drives the proton pump of cytochrome *c* oxidase. *Nature* 440:829–832.
37. Verkhovsky MI, Tuukkanen A, Backgren C, Puustinen A, Wikström M (2001) Charge translocation coupled to electron injection into oxidized cytochrome *c* oxidase from *Paracoccus denitrificans*. *Biochemistry* 40:7077–7083.
38. Verkhovsky MI, Jasaitis A, Verkhovskaya ML, Morgan JE, Wikström M (1999) Proton translocation by cytochrome *c* oxidase. *Nature* 400:480–483.
39. Kucerka N, Tristram-Nagle S, Nagle JF (2006) Closer look at structure of fully hydrated fluid phase DPPC bilayers. *Biophys J* 90:L83–L85.
40. Yoshikawa S, *et al.* (1998) Redox-coupled crystal structural changes in bovine heart cytochrome *c* oxidase. *Science* 280:1723–1729.
41. Takahashi R, Noguchi T (2007) Criteria for determining the hydrogen-bond structures of a tyrosine side chain by Fourier transform infrared spectroscopy: Density functional theory analyses of model hydrogen-bonded complexes of p-cresol. *J Phys Chem B* 111:13833–13844.
42. Lepp H, Svahn E, Faxen K, Brzezinski P (2008) Charge transfer in the k proton pathway linked to electron transfer to the catalytic site in cytochrome *c* oxidase. *Biochemistry* 47:4929–4935.
43. Riistama S, Laakkonen L, Wikström M, Verkhovsky MI, Puustinen A (1999) The calcium binding site in cytochrome aa(3) from *Paracoccus denitrificans*. *Biochemistry* 38:10670–10677.
44. Siletsky SA, *et al.* (2007) Time-resolved single-turnover of ba(3) oxidase from *Thermus thermophilus*. *Biochim Biophys Acta* 1767:1383–1392.
45. Rich PR, Breton J (2002) Attenuated total reflection Fourier transform infrared studies of redox changes in bovine cytochrome *c* oxidase: Resolution of the redox Fourier transform infrared difference spectrum of heme a(3). *Biochemistry* 41:967–973.
46. Verkhovsky MI, Morgan JE, Verkhovskaya ML, Wikström M (1997) Translocation of electrical charge during a single turnover of cytochrome *c* oxidase. *Biochim Biophys Acta* 1318:6–10.
47. Humphrey W, Dalke A, Schulten K (1996) VMD: Visual molecular dynamics. *J Mol Graphics* 14:33–38.